

# Reconfigurable Intelligent Surface Empowered Terahertz Communication for LEO Satellite Networks

Kürşat Tekbiyık, *Student Member, IEEE*, Güneş Karabulut Kurt, *Senior Member, IEEE*, Ali Rıza Ekti, *Member, IEEE*, Ali Görçin, *Senior Member, IEEE*, Halim Yanikomeroglu, *Fellow, IEEE*

**Abstract**—The revolution in the low earth orbit (LEO) satellite networks will impose changes on their communication models, shifting from the classical bent-pipe architectures to more sophisticated networking platforms. Triggered by the technological advancements in the microelectronics and micro-systems, the terahertz (THz) band emerges as a strong candidate for the associated inter-satellite link (ISL) due to its high data rate promise. Yet, the propagation conditions of the THz band need to be properly modeled and/or controlled by utilizing reconfigurable intelligent surfaces (RISs) to assess their full potential. In this work, we first provide an assessment of the use of THz for the ISL, and quantify the impact of the misalignment fading on the error performance. Then, to compensate for the high path loss associated with the high carrier frequencies, we propose the use of RISs that are mounted on the neighboring satellites to enable signal propagation and to further improve the signal-to-noise ratio (SNR). Based on the mathematical analysis of the problem, we present the closed-form error rate expressions for RIS-assisted ISLs under misalignment fading. Numerical results demonstrate that the proposed RIS empowered THz communication solution reveals significant performance improvement introduced by the usage of RIS.

**Index Terms**—Inter-satellite links (ISLs), low earth orbit (LEO) satellite networks, terahertz (THz) band, reconfigurable intelligent surfaces (RISs).

## I. INTRODUCTION

Due to today's space technologies, satellite production and deployment costs are significantly reduced. As a result, low earth orbit (LEO) satellites are becoming an attractive approach for ubiquitous and low-latency communications [1]. The unprecedented growth in LEO satellite deployments open new horizons for the wireless communication world. For example, SpaceX, which plans to locate thousands of satellites in LEO and lower orbits to cover the vast majority of the world's population, aims for seamless and low latency communication between satellites to enable the ubiquitous connection [2].

K. Tekbiyık and G.K. Kurt are with the Department of Electronics and Communications Engineering, Istanbul Technical University, Istanbul, Turkey, e-mails: {tekbiyık, gkurt}@itu.edu.tr

K. Tekbiyık, A.R. Ekti, and A. Görçin are with Informatics and Information Security Research Center (BİLGEM), TÜBİTAK, Kocaeli, Turkey, e-mails: {kursat.tekbiyık, aliriza.ekti, ali.gorcın}@tubitak.gov.tr

A.R. Ekti is with the Department of Electrical–Electronics Engineering, Balıkesir University, Balıkesir, Turkey, e-mail: arekti@balikesir.edu.tr

A. Görçin is with the Department of Electronics and Communications Engineering, Yıldız Technical University, Istanbul, Turkey, e-mail: agorcın@yildiz.edu.tr

H. Yanikomeroglu is with the Department of Systems and Computer Engineering, Carleton University, Ottawa, Canada, e-mail: halim@sce.carleton.ca

To satisfy these demands, flexible connectivity solutions, new types of satellites supporting cooperation in satellites and multi-band are needed. Furthermore, it is envisioned that small satellites will be key drivers for the space communications owing to low production and deployment costs considering the cost of moving a satellite to orbit [3]. Therefore, the requirements for satellite communications need to be revised and redefined to suit small satellites with relatively low power transmission capacities. At this point, it can be considered that using terahertz (THz) waves in inter-satellite links (ISLs) will be a solution for both frequency scarcity and high data rate needs [4]. However, the measurement results show that THz waves suffer from severe path loss [5, 6]. Fortunately, the main contribution to loss due to molecular absorption is not matter for the space applications of THz waves. Even so, the presence of the misalignment between transmitter and receiver antennas dramatically decreases the received power as shown in [7, 8] due to their narrow beams and high directivity. Taking the transmission power limits of LEO satellites into account, utilizing the software-controlled surfaces can satisfy the requirements of the energy-efficient communication framework for THz links [9]. Recently, transmission through reconfigurable intelligent surfaces (RISs) has been proposed as a novel communication technology with a high potential [10]. A RIS consists of many passive elements on top of a plane and it allows to shape of the propagation medium by altering the phase shifts of each element intelligently. The main advantage of the RISs is their operations without active elements, which requires power, whereas multiple-input multiple-output (MIMO) and relay-based approaches employ active elements. Furthermore, the RISs do not need complex processing, and coding [11]. In this respect, it is very suitable for small satellites with low power consumption requirements. As detailed in [12], RISs can provide energy efficiency for the same quality of service (QoS) level. Due to the energy efficiency and low complexity provided by RIS, their use is expected to be a game-changer with THz waves for small satellites of the future.

In this study, RIS-assisted THz band ISLs in LEO constellations, as depicted in Fig. 1, are investigated to meet the requirements such as low-latency, ubiquitous connectivity, high data rate, and low-complexity. Besides, RISs can allow flexibility in the possible transmission direction, which is originally restricted with four nearby satellites in Starlink constellations [13]. Considering this, we propose the cooperation

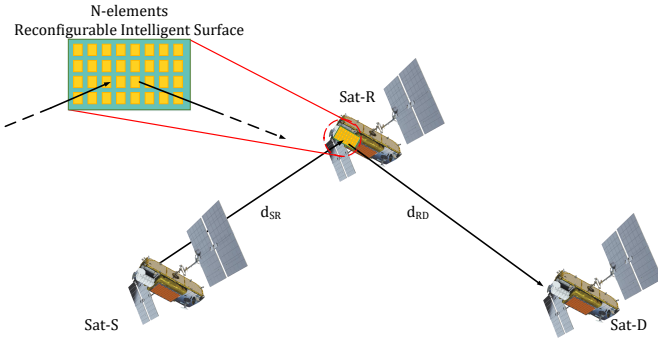


Fig. 1. The system model of a RIS-empowered ISL. The distance between the source (Sat-S) and the relay (Sat-R) is  $d_{SR}$ . Sat-R is equipped with a RIS that is composed of  $N$  elements. The distance between the relay and the destination (Sat-D) is  $d_{RD}$ .

between RIS-assisted satellites in both the same orbit and nearby orbits, and derive the error performance expressions to assess the potential of cooperative techniques in RIS-assisted THz ISLs and validate them with simulation results.

#### A. Contributions

The use of RIS-empowered THz band in LEO satellite ISLs is a promising tool to address high power consumption and low diversity order problems of a single ISL. The contributions of this study is summarized as below:

*Contribution 1:* In this study, the use of RIS in THz communication systems is recommended. This will enable the efficient transmission of the THz waves, which suffer from a high path loss. As shown in [14], the effective path loss exponent can be reduced by the use of RISs in wireless communication links.

*Contribution 2:* Firstly, we focus on the single RIS-assisted THz ISLs to enhance the power efficiency of the LEO satellite networks, as well as to improve the achievable data rates. Furthermore, we consider the misalignment fading, which will be observed in high velocity satellite systems utilizing narrow THz beams, in the performance analysis.

*Contribution 3:* The satellite networks seem to include a massive number of satellites and CubeSats. For example, SpaceX is planning to deploy 1600 satellites for Starlink's initial phase and, SpaceX additionally proposes launching extra 7518 satellites in the orbit with an altitude of 340 km [15]. A cooperative communication paradigm seems to be appropriate for more efficient and effective use of a network with such a large number of satellites. Therefore, utilizing RIS-assisted THz satellite networks in a cooperative manner is addressed in this study. It is shown that benefiting from the cooperation of multiple satellites enhances the power efficiency for a constant bit error probability.

*Contribution 4:* Considering Starlink and Iridium as two sample systems, the performance analysis is carried out in deference to their specifications given in Table I. Thus, the performance results regarding the cases that Starlink and Iridium satellite networks employ the proposed communication framework which utilizes RISs and THz signaling in ISLs are revealed.

#### B. Outline

The rest of this paper is organized as follows. In Section II, we introduce the associated model of the ISLs in LEO constellations in which intra-plane and inter-plane distance models are overviewed. The communication model of the RIS-assisted THz ISL links is given in Section III. The misalignment fading model is given. Single RIS-assisted and multiple RIS-assisted communication scenarios are considered. The associated closed form error expressions are derived. Extensive numerical results and observations are presented in Section IV. Both single and multiple RIS aided cooperation scenarios are considered. In Section V, the conclusions are drawn along with a brief discussion of the related open issues.

### II. INTER-SATELLITE LINKS IN LEO CONSTELLATION

Spreading THz waves in space causes a non-negligible loss in the received power, so the distance between the receiver and the transmitter is the most determining parameter of the loss, which is proportional to the square of the distance. Thus, we firstly find the probable distances between two satellites in both Starlink and Iridium constellations, which are selected as sample networks for this study.

According to the target constellations, the LEO satellites can be positioned at different distances, possible far away from each other. The possible inter-satellite distances can be investigated in three cases: time-invariant distances between two neighboring satellites in the same orbit (Fig. 2(a)), the nearest distance when one of the satellites is located just over one of the poles (Fig. 2(b)), the farthest distance when one of the satellites is just over the equator (Fig. 2(c)) [16]. It is obvious that any possible distance between two satellites in nearby orbits lies in between  $d_{nearest}$  and  $d_{farthest}$ . The first three cases are investigated below. In this study, two extreme cases are investigated to reveal the performance limits. Throughout the study,  $d_{intra}$ ,  $d_{nearest}$ , and  $d_{farthest}$  stand for the inter-satellite distance for an orbit, the shortest and longest distances in between two satellites in nearby orbits, respectively.

#### A. Intra-plane Case

The satellites in the same orbit follow each other with the same distance as shown in Fig. 2(a). The distance from the Earth center to the satellite, with the Earth radius  $r_e$ , is shown by  $r_e + r_s$ . The angle between two neighboring satellites in the same orbit,  $\theta = \frac{360^\circ}{N_{sat}}$ , where  $N_{sat}$  represents the total number of satellites in the orbit. Since the distances to Earth center are the same for each satellite, the angle between the line from center to satellite and the satellite to satellite line is calculated by

$$\varphi = \frac{180^\circ - \theta}{2}. \quad (1)$$

By using the law of sines,

$$d_{intra} = \frac{(r_e + r_s) \times \sin(\theta)}{\sin(\varphi)}, \quad (2)$$

where  $d_{intra}$  denotes the distance between two neighbor satellites in the same orbit.

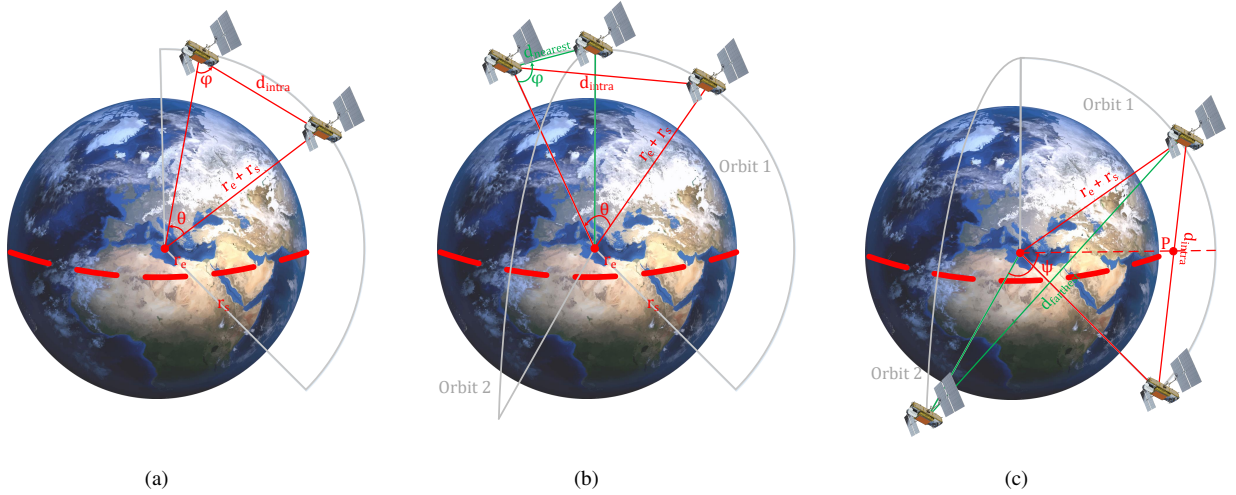


Fig. 2. Satellites can be located in various positions in orbits relative to each other. Three of them are: (a) intra-plane distance, (b) the nearest, and (c) the farthest. While the distance between the satellites in the same orbit is constant throughout the movement, the distance between the satellites in the two neighboring orbits changes with time. Two extreme examples of the nearest and farthest are shown.

### B. Inter-plane Case

In this section, the minimum and maximum distances between satellites in the nearby orbits are investigated to reveal the upper and lower limits.

1) *The Nearest Case:* Where two satellites in different orbits are closest to each other, one of the satellites is directly above the north or south pole. It should be noted at this point that although Starlink satellites do not pass exactly over the pole points, it is worth to say that, for example, the north-east orbits form virtual poles above the north and south 53rd-degree latitudes. This scenario is illustrated in Fig. 2(b). Likewise the intra-plane case, the nearest distance is found by applying the law of sines as

$$d_{\text{nearest}} = \frac{(r_e + r_s) \times \sin(\frac{\theta}{2})}{\sin(\varphi)}, \quad (3)$$

where  $\frac{\theta}{2}$  and  $\varphi = \frac{180-\theta/2}{2}$  are half of the angle between the line from center to satellite and the angle between the inter-satellite line and the line through the center of the Earth, respectively.

2) *The Farthest Case:* When the satellite positions at just over the equator, the distance to the satellite in neighbor orbit becomes maximum as seen in Fig. 2(c). The distance from the center of Earth to the point  $P$  is calculated by using Pythagoras theorem as

$$|OP| = \sqrt{(r_e + r_s)^2 - \left(\frac{d_{\text{intra}}}{2}\right)^2}. \quad (4)$$

Then, the distance between the satellite in orbit 2 and the point  $P$  is

$$d_{\text{SP}} = \sqrt{(r_e + r_s)^2 + |OP|^2 - 2(r_e + r_s)|OP| \cos(\Psi)} \quad (5)$$

where  $\Psi$  is the angle between two nearby orbits. Therefore,  $\Psi$  is equal to  $\frac{180^\circ}{N_{\text{orbit}}}$  for a constellation with  $N_{\text{orbit}}$  orbits. Finally, the farthest distance between satellites is deduced as

$$d_{\text{farthest}} = \sqrt{d_{\text{SP}}^2 + \left(\frac{d_{\text{intra}}}{2}\right)^2}. \quad (6)$$

TABLE I

THE DISTANCES FOR IRIDIUM AND STARLINK CONSTELLATIONS.

Specifications	Iridium	Starlink*
$r_s$ (km)	781	1150
$N_{\text{sat}}$	11	50
$N_{\text{orbit}}$	6	32
$\theta$	32.73°	7.2°
$\Psi$	30°	5.625°
$d_{\text{intra}}$ (km)	4034	945.4
$d_{\text{nearest}}$ (km)	2037.8	472.93
$d_{\text{farthest}}$ (km)	4162.8	876.57

\*The values are given according to the first phase of Starlink.

As an example, the distances are shown in Table I for the two example satellite constellations: Starlink and Iridium. Since Starlink has more orbits and satellites per orbit, the distances are relatively short compared to Iridium satellite network.

### III. RIS-ASSISTED TERAHERTZ WIRELESS COMMUNICATION IN INTER-SATELLITE LINKS

In this section, RIS-assisted THz ISLs are considered under the misalignment fading due to sharp beams of THz antennas and high relative velocity of LEO satellites. To the best knowledge of the authors, this study provides error performance analysis for RIS-assisted THz ISLs in LEO satellite networks for the first time in the literature.

#### A. Misalignment Fading

Since THz antennas creates pencil sharp beams and the motion of LEO satellites with high velocity around  $28 \times 10^3$  kph, the possible misalignment fading should be considered in THz-empowered ISLs. Under the circular beam assumption, considering beams with the radial distance,  $r$ , between their centers on the x-y plane, the misalignment coefficient  $\zeta$  can be expressed as [17]

$$\zeta(r; d) \approx A_o \exp\left(-\frac{2r^2}{w_{eq}^2}\right), \quad (7)$$

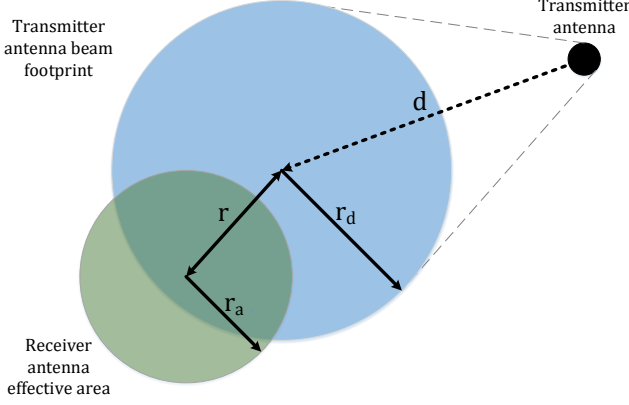


Fig. 3. The beam misalignment illustration for the receiver's effective area with radius  $r_a$  and the transmitter's beam footprint at distance  $d$  shown by  $r_d$  when the presence of the pointing error  $r$ .

where

$$A_0 = \left[ \operatorname{erf} \left( \frac{\sqrt{\pi} r_a}{\sqrt{2} r_d} \right) \right]^2, \quad (8)$$

$$w_{eq}^2 = r_d^2 \frac{\operatorname{erf} \left( \frac{\sqrt{\pi} r_a}{\sqrt{2} r_d} \right)}{\frac{\sqrt{2} r_a}{r_d} \exp \left( -\frac{\pi r_a^2}{2 r_d^2} \right)}.$$

$A_0$ ,  $w_{eq}$ , and  $r_d$  denote the collected power fraction in the aligned case (i.e.,  $r = 0$ ), equivalent beam width, and the beam waist at distance  $d$ , respectively.  $r_a$  is the radius of the receiver antenna effective area, which under the circular area assumption, it can be expressed by modifying antenna aperture area equation [18] as follows

$$A_e = \pi r_a^2 = \frac{\lambda^2}{4\pi} G, \quad (9)$$

then,

$$r_a = \frac{\lambda}{2\pi} \sqrt{G}, \quad (10)$$

where  $G$  denotes the antenna gain. Due to the fact that the displacement in both directions follow independent identical Gaussian distribution, the radial distance,  $r$ , can be modeled by Rayleigh distribution as

$$f_r(r) = \frac{r}{\sigma_s^2} \exp \left( -\frac{r^2}{2\sigma_s^2} \right), \quad r > 0, \quad (11)$$

where  $\sigma_s^2$  stands for the receiver's jitter variance. By jointly utilizing (7) and (11), the misalignment fading is introduced as follows

$$f_\zeta(y) = \frac{\kappa^2}{A_0^{\kappa^2}} y^{\kappa^2-1}, \quad 0 \leq y \leq A_0, \quad (12)$$

where  $\kappa = \frac{w_{eq}^2}{2\sigma_s^2}$  [19]. Thus, jitter variance appears as an important parameter affecting communication performance.

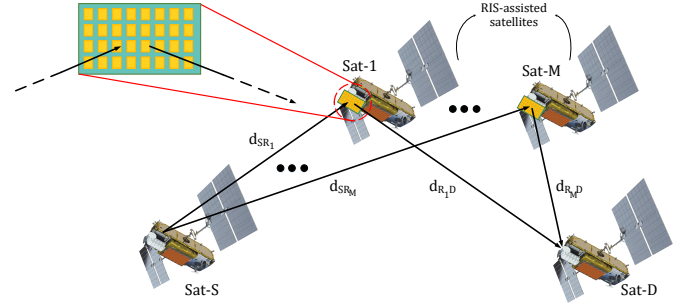


Fig. 4. The illustration for the simultaneous multiple RIS-assisted satellite communication framework consisting a source (Sat-S), destination (Sat-D), and  $M$  satellites equipped with RIS.

### B. Single RIS-assisted Wireless Channel and Associated Performance Analysis

Under the flat fading assumption, the signal received by the destination node for  $N$ -element RIS is expressed as follows

$$r = \sqrt{p_t P_L} \left( \sum_{i=1}^N \rho_i^{SR} e^{j\phi_i} \rho_i^{RD} \zeta_i^{SR} \zeta_i^{RD} \right) x + n, \quad (13)$$

where  $\rho_i^{SR}$  and  $\rho_i^{RD}$  denote the channel impulse responses. The phase shift adjusted by  $i$ th element of RIS is represented by  $\phi_i$ .  $x$  is the data symbol from possible constellation of an  $M$ -ary phase shift keying (PSK) or quadrature amplitude modulation (QAM).  $n$  is zero-mean complex additive white Gaussian noise (AWGN) with variance of  $N_0$ .  $\phi_i$  is the adjustable phase shifts created by the  $i$ th-elements of RIS.  $\zeta_i^{SR}$  and  $\zeta_i^{RD}$  stand for the misalignment fading in the links source-to-RIS and RIS-to-destination. Also,  $p_t$  and  $P_L$  are the transmit power of source and the total path loss through the path propagating by the signal, respectively. The total path length is  $d_{SR}^2 + d_{RD}^2$  in the near-field behavior; however, it becomes  $d_{SR}^2 \times d_{RD}^2$  under the far-field of RIS [20]. The path loss in the free-space is expressed as

$$P_L = \left( \left( \frac{\lambda}{4\pi} \right)^4 \frac{G_i G_r}{d_{SR}^2 d_{RD}^2} \epsilon_p \right)^{-1}, \quad (14)$$

where  $G_i$  and  $G_r$  are gains in the direction of incoming and receiving waves, which are chosen as 30 dBi for 350 GHz operating frequency as given in [21].  $\lambda$  denotes the wavelength corresponding to propagation frequency of wave,  $\epsilon_p$  stands for the efficiency of RIS. For the lossless RIS,  $\epsilon_p$  is equal to 1.

By rewriting the channel impulse responses in terms of channel amplitudes and phases as  $\rho_i^{SR} = \alpha_i^{SR} e^{-j\beta_i^{SR}}$  and  $\rho_i^{RD} = \alpha_i^{RD} e^{-j\beta_i^{RD}}$ , (15) can be expressed as follows

$$r = \sqrt{p_t P_L} \left( \sum_{i=1}^N \alpha_i^{SR} \alpha_i^{RD} e^{j(\phi_i - \beta_i^{SR} - \beta_i^{RD})} \zeta_i^{SR} \zeta_i^{RD} \right) x + n. \quad (15)$$

Then, the instantaneous signal-to-noise ratio (SNR) observed at the receiver as

$$\gamma = \frac{p_t \left| \sqrt{P_L} \left( \sum_{i=1}^N \alpha_i^{SR} \alpha_i^{RD} e^{j\psi} \zeta_i^{SR} \zeta_i^{RD} \right) \right|^2}{N_0}, \quad (16)$$



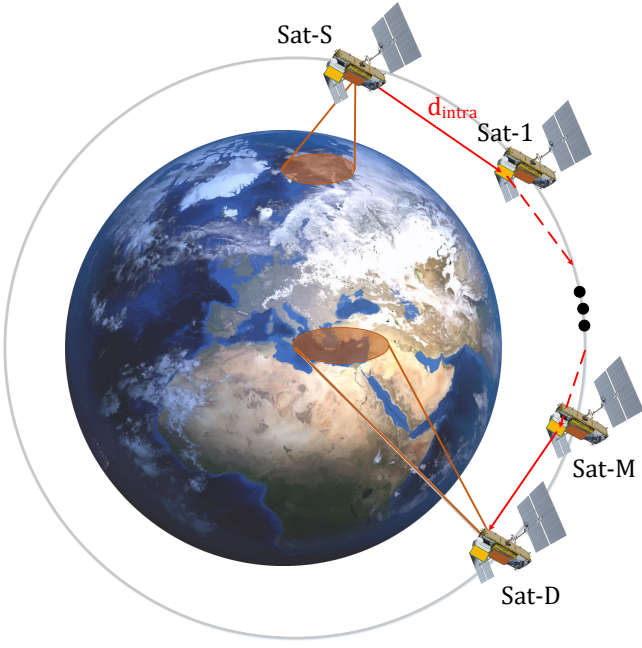


Fig. 5. The illustration for the consecutive multiple RIS-assisted satellite communication framework consisting a source (Sat-S), destination (Sat-D), and  $M$  satellites equipped with RIS, which are in the same orbit.

where  $\psi = \phi_i - \beta_i^{SR} - \beta_i^{RD}$  and it is zero for the maximum instantaneous SNR as

$$\gamma_{\max} = \frac{p_t \left| \sqrt{P_L} \left( \sum_{i=1}^N \alpha_i^{SR} \alpha_i^{RD} \zeta_i^{SR} \zeta_i^{RD} \right) \right|^2}{N_0} = \frac{A^2 p_t}{N_0}, \quad (17)$$

where  $\alpha_i^{SR}$  and  $\alpha_i^{RD}$  follow the Rician distribution which is possibly observed in the space communication due to the presence of high power line of sight (LOS) link with non-line of sight (NLOS) links reflected from other space things.  $\zeta_i^{SR}$  and  $\zeta_i^{RD}$  are the misalignment fading coefficients following the distribution given in (12). According to the central limit theorem (CLT), variable  $A$  follows the Gaussian distribution for  $N \gg 1$  with the mean and variance given in (18), where  $L_{1/2}(\cdot)$  stands for the Laguerre polynomials of degree 1/2. As  $A$  follows the Gaussian distribution, SNR is non-central chi-square distributed with one degree of freedom. To evaluate the bit error probability (BEP), the moment generating function (MGF) of non-central chi-square distribution [22] is utilized as given in (19). By utilizing the symbol error probability (SEP) expression for  $M$ -PSK signals given in [23], the error probability for binary phase shift keying (BPSK) is obtained as in (20). It implies that the error probability degrades inversely  $N^2$  while it proportionally increases with  $(\sigma_s^2)^4$  due to the term  $\kappa$  in the equation.

### C. Multiple RIS-assisted Wireless Channel and Associated Performance Analysis

In this section, we investigate the performance for the multiple RIS-assisted satellite networks. Firstly, likewise [14], we derive a mathematical expression of the error probability

for a simultaneous transmission over  $M$  independent RISs. Then, we analyse the error performance for the transmission path consisting  $M$  reflections over consecutive RISs.

1) *Simultaneous Transmission over  $M$  independent RISs:* For the scenario depicted in Fig. 4, the received signal can be expressed as

$$r = \sqrt{p_t} \left[ \sum_{k=1}^M \sqrt{P_{Lk}} \left( \sum_{i=1}^{N_k} \alpha_i^{SR_k} \alpha_{i,k}^{R_k D} e^{j\psi_k} \zeta_{i,k}^{SR_k} \zeta_{i,k}^{R_k D} \right) \right] x + n, \quad (21)$$

where each element of equation is the same as in (15) for  $k$ -th RIS. Similarly (22), the maximum instantaneous SNR is given as

$$\begin{aligned} \gamma_{\max} &= \frac{p_t \left| \sum_{k=1}^M \left[ \sqrt{P_{Lk}} \left( \sum_{i=1}^{N_k} \alpha_i^{SR_k} \alpha_{i,k}^{R_k D} \zeta_{i,k}^{SR_k} \zeta_{i,k}^{R_k D} \right) \right] \right|^2}{N_0} \\ &= \frac{A^2 p_t}{N_0}. \end{aligned} \quad (22)$$

By taking CLT into account for  $N_k \gg 1, \forall k = 1, 2, \dots, M$ , it can be said that  $A$  follows Gaussian distribution with the mean and variance given as in (23). Similar to the single RIS-assisted communication performance analysis, we can derive the error probability as stated in (24), which implies that the error performance increases in proportion to the square of the total reflective elements in accordance with [14].

2) *Transmission over  $M$  Consecutive RIS-assisted Satellites:* The double-RIS reflected transmission proposed in [14] is generalized for  $M$  consecutive RIS reflections as depicted in Fig. 5. Considering the baseband equivalent received signal given in [14], we can generalize the received signal passing through a path consisting  $M$  consecutive RIS reflections as follows

$$r = \sqrt{p_t P_L} \left[ \sum_{i_1=1}^N \sum_{i_2=1}^N \cdots \sum_{i_M=1}^N \alpha_{i_1 \dots i_M} e^{j\psi} \right] x + n, \quad (25)$$

where  $\alpha_{i_1 \dots i_M}$  and  $\psi$  denote the overall channel amplitude and overall channel phase along with the reconfiguration phases of RISs. It should be noticed that the transmitter and receiver are fully aligned in this case. Configuring as  $\psi = 0$ , the maximum instantaneous SNR is obtained as

$$\begin{aligned} \gamma_{\max} &= \frac{p_t \left| \sqrt{P_L} \left[ \sum_{i_1=1}^N \sum_{i_2=1}^N \cdots \sum_{i_M=1}^N \alpha_{i_1 \dots i_M} \right] \right|^2}{N_0} \\ &= \frac{A^2 p_t}{N_0}. \end{aligned} \quad (26)$$

For  $N \gg 1$ ,  $A$  follows Gaussian distribution with mean and variance given as

$$\begin{aligned} \mathbb{E}[A] &= \frac{N^M \sqrt{P_L \pi}}{\sqrt{4(1+K)}} L_{1/2}(-K), \\ \text{Var}[A] &= N^M P_L \left( 1 - \frac{\pi}{4(1+K)} (L_{1/2}(-K))^2 \right). \end{aligned} \quad (27)$$

$$\begin{aligned}\mathbb{E}[A] &= \frac{N\sqrt{P_L}}{2(1+K)} \frac{\pi}{2} (L_{1/2}(-K))^2 \frac{\kappa^4}{(\kappa^2+1)^2} A_0^2, \\ \text{Var}[A] &= NP_L \left( A_0^4 \frac{\kappa^4}{(\kappa^2+2)^2} - \left[ \frac{\pi}{4(1+K)} (L_{1/2}(-K))^2 \frac{\kappa^4}{(\kappa^2+1)^2} A_0^2 \right]^2 \right)\end{aligned}\quad (18)$$

$$M_{\gamma_{max}}(s) = \frac{\exp\left(-\frac{\frac{P_t}{N_0} \frac{N^2 P_L \pi^2}{16(1+K)^2} (L_{1/2}(-K))^4 \frac{\kappa^8}{(\kappa^2+1)^4} A_0^4}{1-2s \frac{P_t}{N_0} NP_L \left(\frac{A_0^4 \kappa^4}{(\sigma^2+2)^2} - \left[\frac{\pi}{4(1+K)} (L_{1/2}(-K))^2 \frac{\kappa^4}{(\kappa^2+1)^2} A_0^2\right]^2\right)}\right)}{\sqrt{1-2s \frac{P_t}{N_0} NP_L \left(\frac{A_0^4 \kappa^4}{(\kappa^2+2)^2} - \left[\frac{\pi}{4(K+1)} (L_{1/2}(-K))^2 \frac{\kappa^4}{(\kappa^2+1)^2} A_0^2\right]^2\right)}}.\quad (19)$$

$$P_e = \frac{1}{\pi} \int_0^{\pi/2} \frac{\exp\left(-\frac{\frac{P_t}{N_0} \frac{N^2 P_L \pi^2}{16(1+K)^2} (L_{1/2}(-K))^4 \frac{\kappa^8}{(\kappa^2+1)^4} A_0^4}{1+2\sin^2(\omega) \frac{P_t}{N_0} NP_L \left(\frac{A_0^4 \kappa^4}{(\sigma^2+2)^2} - \left[\frac{\pi}{4(1+K)} (L_{1/2}(-K))^2 \frac{\kappa^4}{(\kappa^2+1)^2} A_0^2\right]^2\right)}\right)}{\sqrt{1+2\sin^2(\omega) \frac{P_t}{N_0} NP_L \left(\frac{A_0^4 \kappa^4}{(\kappa^2+2)^2} - \left[\frac{\pi}{4(K+1)} (L_{1/2}(-K))^2 \frac{\kappa^4}{(\kappa^2+1)^2} A_0^2\right]^2\right)}} d\omega.\quad (20)$$

$$\begin{aligned}\mathbb{E}[A] &= \left(\sum_{k=1}^M N_k \sqrt{P_{Lk}}\right) \times \frac{\pi}{4(1+K)} (L_{1/2}(-K))^2 \frac{\kappa^4}{(\kappa^2+1)^2} A_0^2, \\ \text{Var}[A] &= \left(\sum_{k=1}^M N_k P_{Lk}\right) \times \left( A_0^4 \frac{\kappa^4}{(\kappa^2+2)^2} - \left[ \frac{\pi}{4(1+K)} (L_{1/2}(-K))^2 \frac{\kappa^4}{(\kappa^2+1)^2} A_0^2 \right]^2 \right)\end{aligned}\quad (23)$$

$$P_e = \frac{1}{\pi} \int_0^{\pi/2} \frac{\exp\left(-\frac{\left(\sum_{k=1}^M N_k \sqrt{P_{Lk}}\right)^2 \frac{P_t}{N_0} \frac{\pi^2}{16(1+K)^2} (L_{1/2}(-K))^4 \frac{\kappa^8}{(\kappa^2+1)^4} A_0^4}{1+2\sin^2(\omega) \frac{P_t}{N_0} \left(\sum_{k=1}^M N_k P_{Lk}\right) \left(\frac{A_0^4 \kappa^4}{(\sigma^2+2)^2} - \left[\frac{\pi}{4(1+K)} (L_{1/2}(-K))^2 \frac{\kappa^4}{(\kappa^2+1)^2} A_0^2\right]^2\right)}\right)}{\sqrt{1+2\sin^2(\omega) \frac{P_t}{N_0} \left(\sum_{k=1}^M N_k P_{Lk}\right) \left(\frac{A_0^4 \kappa^4}{(\kappa^2+2)^2} - \left[\frac{\pi}{4(K+1)} (L_{1/2}(-K))^2 \frac{\kappa^4}{(\kappa^2+1)^2} A_0^2\right]^2\right)}} d\omega.\quad (24)$$

By applying same procedure as in Section III-C1, the error probability is obtained as

$$P_e = \frac{1}{\pi} \int_0^{\pi/2} \frac{\exp\left(-\frac{\frac{N^2 M P_L \pi}{4(1+K) L_{1/2}^2(-K)}}{1+2 \frac{N^M P_L}{\sin^2(\omega)} \left(1 - \frac{\pi}{4(1+K)} L_{1/2}^2(-K)\right)}\right)}{\sqrt{1+2 \frac{N^M P_L}{\sin^2(\omega)} \left(1 - \frac{\pi}{4(1+K)} L_{1/2}^2(-K)\right)}} d\omega.\quad (28)$$

#### IV. NUMERICAL RESULTS AND DISCUSSION

In this section, the numerical results regarding theoretical findings in Section III. It should be noted that during the studies carried out in this section, the operating frequency of the system has been determined as 350 GHz and the gain value for the antenna operating in frequency is 30 dBi given in [21]. As mentioned, the channel amplitude coefficients follow Rician distribution with parameter  $K = 10$ . First

of all, we investigate the error performance for single RIS-assisted satellite constellations. Then, multiple RIS employed in the satellite networks, and the communication performance analyses are carried out regarding these scenarios.

##### A. Single RIS-assisted THz Inter-satellite Links

Firstly, THz ISLs over a single RIS is considered as depicted in Fig. 1. In this case, there is no direct link between the source and destination satellites, which is an acceptable assumption considering the satellite constellations [15]. Due to fast relative velocity and possible beam tracking errors, the misalignment fading is required to be considered. Hence, in this section, the misalignment fading is investigated for RIS-assisted THz satellite networks. To the best knowledge of the authors, this study firstly considers the misalignment fading in RIS-assisted THz communications.

In the study, two basic satellite constellations, Starlink and Iridium, are considered as examples and numerical results

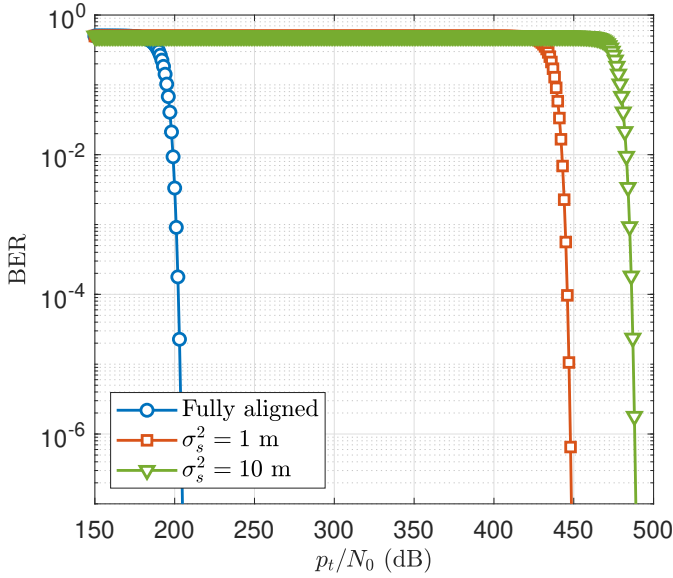


Fig. 6. BER performance of single RIS-assisted Starlink constellation with BPSK signaling over 1024-element RIS for fully aligned transmission and transmission with some jitter variances.

are given over these example satellite network constellations. Basically, the differences between these two constellations result from the number of orbits and satellites in each orbit are given in Table I.

We assume that the distances Sat-S to Sat-R and Sat-R to Sat-D are equal to  $d_{intra}$ , namely it can be thought that they are in the same orbit. For Starlink constellation,  $d_{intra}$  is 945.4 km while Iridium's intra-satellite distance is 4034 km. Firstly, the impact of misalignment fading on the error performance is analysed comparing fully aligned system with some jitter variances. Fig. 6 reveals that in parallel with [24], alignment appears to be critical for THz communication systems.

For varying number of RIS elements, the error performances are depicted in Fig. 7 for the system resembling Starlink constellations. It can be observed that when the number of RIS elements is doubled, 6 dB power is gained to satisfy the same error performance as given in (20). Also, the misalignment fading is investigated in Fig. 7(a) and Fig. 7(b). Firstly,  $\sigma_s^2$  is assumed to be 1 m. Considering the results depicted in both figures, when the jitter variance is increased 10 times, 40 dB more power must be used to ensure the same error performance as shown in (20). These results show that THz satellite networks should either use RIS with higher number of elements or beam tracking methods that work with very low errors at the expense of high computational cost must be adopted. Similar behaviors are observed in Fig. 8 for Iridium constellation but path loss is higher since it has longer intra-satellite distances than Starlink constellation. As a result, more output power is needed to compensate for path loss.

### B. Multiple RIS-assisted THz Inter-satellite Links

By utilizing cooperation in satellite networks since they are planned to be densely connected with each other, multiple satellites equipped with RIS can be employed in the cooperative manner. Thus, the diversity order can escalate. For this

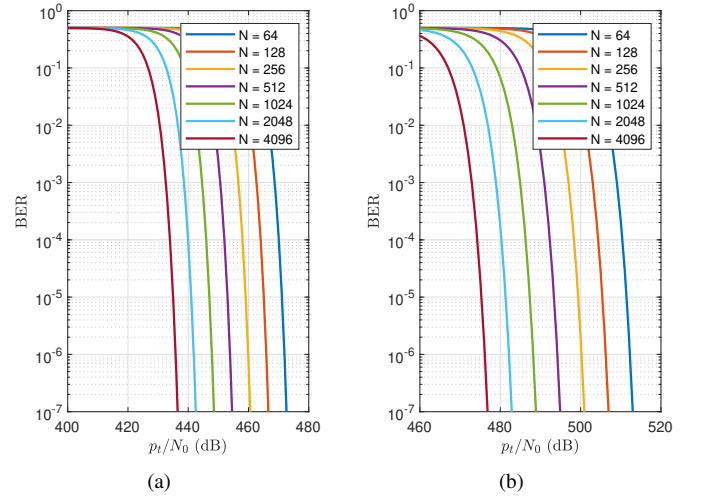


Fig. 7. BER performance of single RIS-assisted Starlink constellation for different RIS sizes under BPSK signaling and the misalignment fading with receiver's jitter variances of (a)  $\sigma_s^2 = 1$  m, (b)  $\sigma_s^2 = 10$  m.

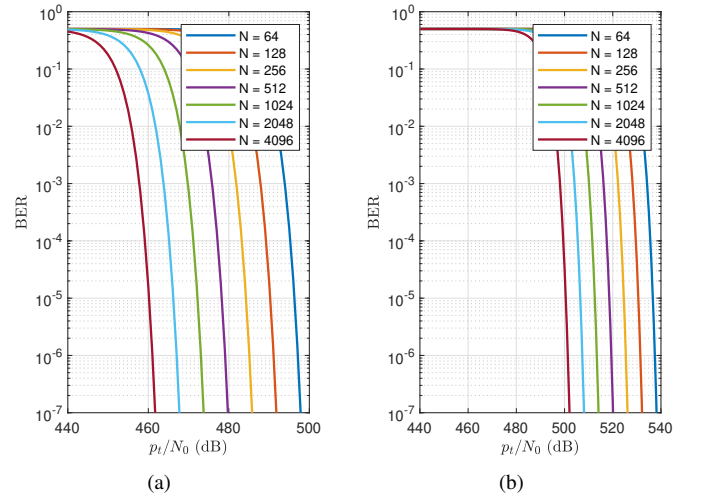


Fig. 8. BER performance of single RIS-assisted Iridium constellation for different RIS sizes under BPSK signaling and the misalignment fading with receiver's jitter variances of (a)  $\sigma_s^2 = 1$  m, (b)  $\sigma_s^2 = 10$  m.

aim, we investigate two different cases. First, simultaneous transmission over multiple satellites and then, transmission over  $M$  consecutive satellites are studied.

1) *Performance Analysis for Simultaneous Transmission over Multiple Satellites:* As depicted in Fig. 4,  $M$  satellites equipped with RIS can simultaneously transmit the incident signal to the destination satellite by increasing diversity order and dropping down the path loss exponent [11]. (24) clearly shows that the error probability is inversely proportional with the square of the total number of RIS elements. It should be noted that in the light of (24), the misalignment fading remains same as single RIS case. In this scenario,  $M$  is selected as 2 with varying number of RIS elements. It is assumed that each distance is equal to  $d_{intra}$ ; hence,  $P_{Lk} = P_L, \forall k = 1, 2$ . Also, the number of RIS element is selected as same. In Fig. 9 and Fig. 10, the error performances are investigated for Starlink and Iridium constellations, respectively. In this case, the error rate is proportional with  $(2N)^{-2}$ . As a result, the same error

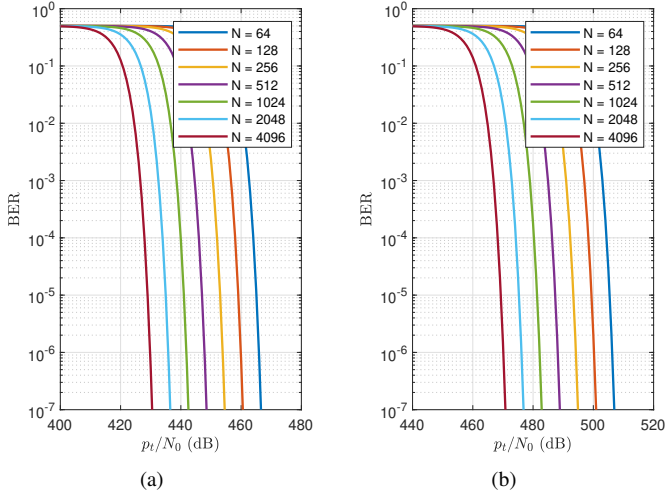


Fig. 9. BER performance of double simultaneous RISs-assisted Starlink constellation for different RIS sizes under BPSK signaling and the misalignment fading with receiver's jitter variances of (a)  $\sigma_s^2 = 1\text{m}$ , (b)  $\sigma_s^2 = 10\text{m}$ . The distances are assumed as  $d_{intra}$ .

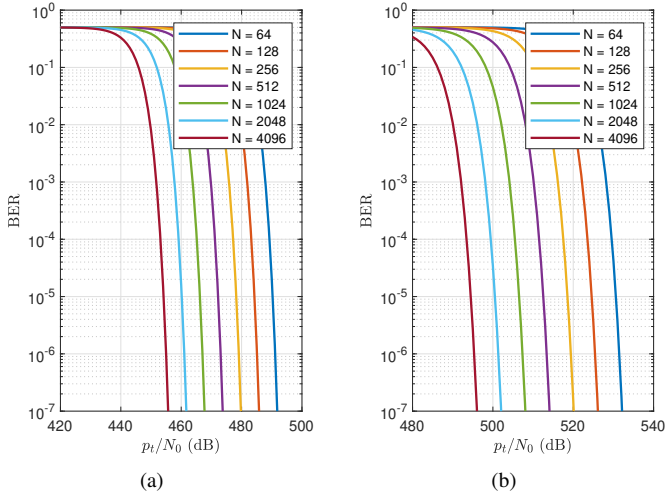


Fig. 10. BER performance of double simultaneous RISs-assisted Iridium constellation for different RIS sizes under BPSK signaling and the misalignment fading with receiver's jitter variances of (a)  $\sigma_s^2 = 1\text{m}$  and (b)  $\sigma_s^2 = 10\text{m}$ . The distances are assumed as  $d_{intra}$ .

rate can be achieved with 6 dB less power compared to single RIS case.

For the achievable rate analysis,  $d_{SR_1}$  and  $d_{R_1D}$  is set to  $d_{intra}$ .  $d_{SR_2}$  and  $d_{R_2D}$  vary from  $d_{nearest}$  to  $d_{farthest}$  to create a scenario such that Sat-S, Sat-1, and Sat-D are consecutive satellites in the same orbit while Sat-2 is in the nearby orbit. Fig. 11 and Fig. 12 denote achievable rate for Starlink and Iridium satellites equipped with 1024-elements RISs for the satellite position between two extreme distances. As expected, the maximum rate is achieved when the distances are minimum. A 10-fold increase in misalignment fading causes the maximum achievable data rate to decrease by 5 bits/s/Hz. For THz band, this decrease cannot be overlooked since the total data rate decrease reaches 300 Gbps for 60 GHz bandwidth. Owing to fact that the path loss between two consecutive satellites in Starlink is less than Iridium network,

the achievable rate for Iridium constellation is less. Considering the cost of construction and maintenance of satellites, increasing the number of satellites in each orbit cannot be feasible. Therefore, increasing the number of RIS elements on each satellite can provide cost-effective solution to reach the desired achievable rate.

2) *Performance Analysis for Transmission over  $M$  Consecutive Satellites*: Finally, the transmission sequentially through satellites scenario in the same orbit is investigated because satellite networks are designed to allow communication between different orbits in a limited way while allowing easy transmission on the same orbit [15]. In this scenario, since all satellites are in the same orbit, the distance between the satellites is constant, so path losses between satellites can be considered equal. It should be noticed that the fully aligned case is considered in this scenario.

As (28) implies that  $P_e \propto N^{2M}$ , increasing number of consecutive satellites significantly improves error performance. For example, increasing from  $M = 2$  to  $M = 4$  results in approximately 120 dB power gain when 1024-element RISs are employed in satellite networks. This result are obviously seen in Fig. 13. As seen in Fig. 13, when the number of RIS elements is doubled, the power gain is 12 dB and 24 dB for  $M = 2$  and  $M = 4$ , respectively. These results indicate that the power gain in transmission along the orbit can increase significantly.

## V. CONCLUSIONS

In this study, a solution to both frequency scarcity and low-complexity system design is proposed by the use of RIS and THz waves together in links between LEO satellites. It is possible to increase the achievable rates due to the ultra-wide bandwidth provided by the THz wave and the RIS acting like N-elements virtual MIMO system. It also appears that error probability decreases inversely proportional to the square of the number of elements of RIS. We consider the misalignment fading, which is possibly faced in the THz LEO satellite networks, in our mathematical expressions, which are validated with simulation results. Our study shows that misalignment between the antennas gives rise to a severe drop in the received power. This indicates that a beam tracker is needed to ensure a convenient alignment system between the antennas. In addition, considering the node density of the next-generation LEO satellites networks, cooperative communication techniques emerge as a promising tool to improve the ISL performances. The performance of simultaneous and consecutive transmission over satellites equipped with more than one RIS is investigated. The derived mathematical expressions and simulation results denote that an increase in the number of RISs can reduce the required transmission power targeting the same error probability.

As a future work, a path that can minimize the target performance metrics, such as the round trip time, can be investigated by using RISs with an optimization framework. Thus, RISs can be used not only to improve communication performance but also to address other requirements, such as reducing the latency between the two nodes. By modeling this



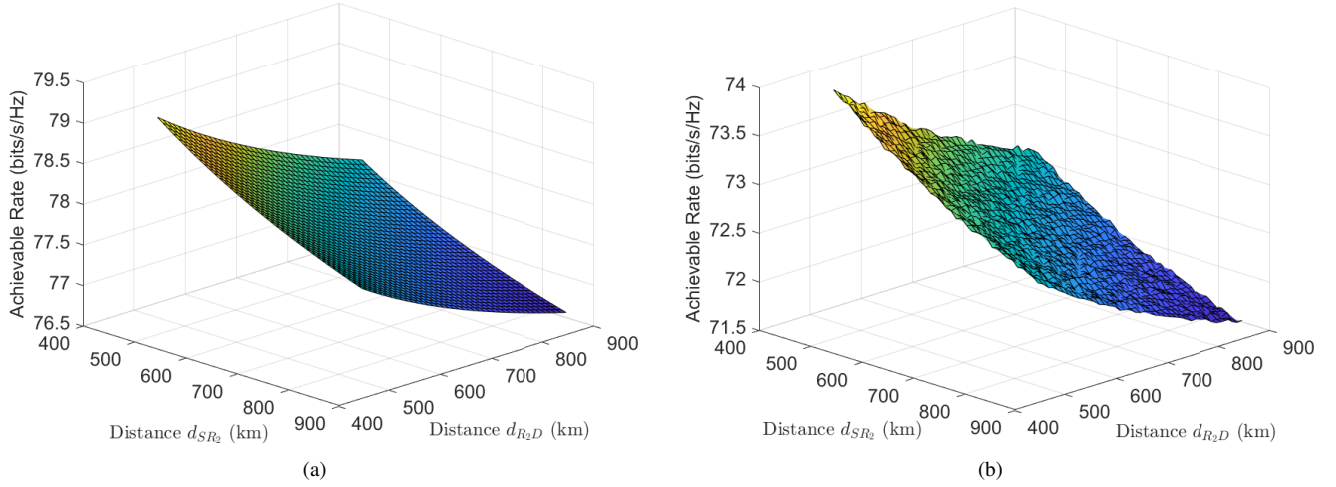


Fig. 11. Achievable data rate performance double simultaneous RISs-assisted Starlink constellation for varying distances (i.e.,  $d_{SR_2}$  and  $d_{R_2D}$ ) from  $d_{nearest}$  to  $d_{farthest}$  under two misalignment cases: (a)  $\sigma_s^2 = 1\text{m}$  and (b)  $\sigma_s^2 = 10\text{m}$  when  $N = 1024$ .  $d_{SR_1}$  and  $d_{R_1D}$  are kept constant as  $d_{intra}$ .

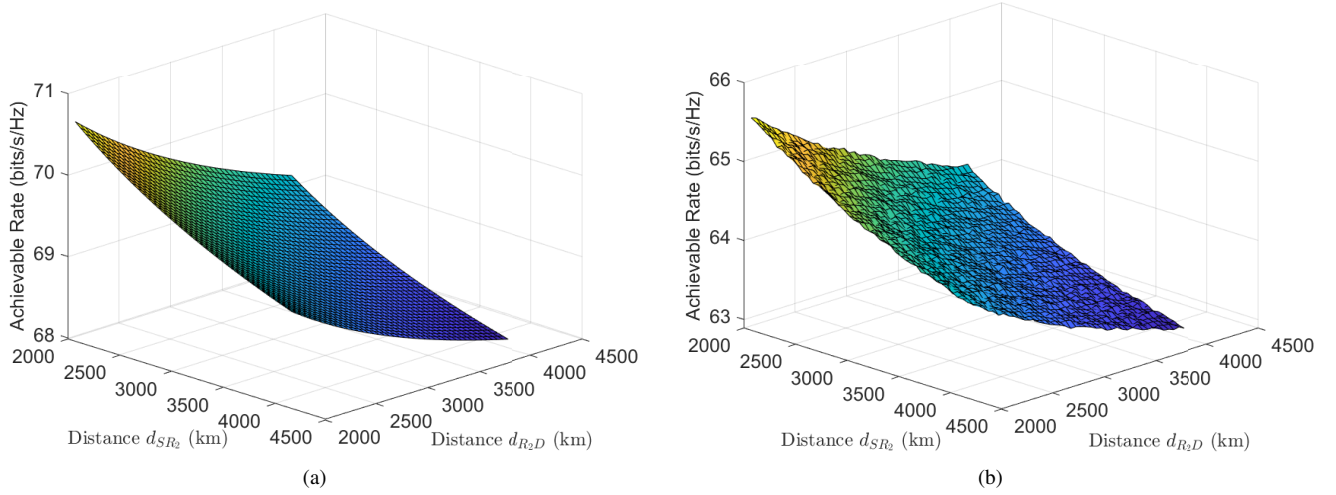


Fig. 12. Achievable data rate performance double simultaneous RISs-assisted Iridium constellation for varying distances (i.e.,  $d_{SR_2}$  and  $d_{R_2D}$ ) from  $d_{nearest}$  to  $d_{farthest}$  under two misalignment cases: (a)  $\sigma_s^2 = 1\text{m}$ , (b)  $\sigma_s^2 = 10\text{m}$  when  $N = 1024$ .  $d_{SR_1}$  and  $d_{R_1D}$  are kept constant as  $d_{intra}$ .

problem as traveling sales man problem, the path satisfying the minimum latency can be solved by the mixed integer nonlinear programming. Furthermore, a performance analysis is needed when satellites move through their orbits, and can be obtained by utilizing orbit modeling tools, such as SaVi.

## REFERENCES

- [1] K. Woellert, P. Ehrenfreund, A. J. Ricco, and H. Hertzfeld, "Cubesats: Cost-effective science and technology platforms for emerging and developing nations," *Advances in Space Research*, vol. 47, no. 4, pp. 663–684, 2011.
- [2] N. Saeed, A. Elzanaty, H. Almorad, H. Dahrouj, T. Y. Al-Naffouri, and M.-S. Alouini, "Cubesat communications: Recent advances and future challenges," *IEEE Commun. Surv. Tutorials*, 2020.
- [3] I. F. Akyildiz and A. Kak, "The Internet of space things/CubeSats," *IEEE Network*, vol. 33, no. 5, pp. 212–218, 2019.
- [4] K. Tekbıyık, A. R. Ekti, G. K. Kurt, A. Görçin, and H. Yanıkömeroğlu, "A holistic investigation on terahertz propagation and channel modeling toward vertical HetNets," *arXiv preprint arXiv:2005.00509*, 2020.
- [5] T. Schneider, A. Wiatrek, S. Preußler, M. Grigat, and R.-P. Braun, "Link budget analysis for terahertz fixed wireless links," *IEEE Trans. Terahertz Sci. Technol.*, vol. 2, no. 2, pp. 250–256, 2012.
- [6] K. Tekbıyık, E. Ulusoy, A. R. Ekti, S. Yarkan, T. Baykaş, A. Görçin, and G. K. Kurt, "Statistical channel modeling for short range line-of-sight terahertz communication," in *30th Annual International Symposium on Personal, Indoor and Mobile Radio Communications (PIMRC)*, 2019, pp. 1–5.
- [7] S. Priebe, M. Jacob, and T. Kürner, "Affection of THz indoor communication links by antenna misalignment," in *6th European Conference on Antennas and Propagation (EUCAP)*, 2012, pp. 483–487.
- [8] A. R. Ekti, A. Boyacı, A. Alparslan, İ. Ünal, S. Yarkan, A. Görçin, H. Arslan, and M. Uysal, "Statistical modeling of propagation channels for terahertz band," in *IEEE Conference on Standards for Communications and Networking (CSCN)*, 2017, pp. 275–280.
- [9] C. Liaskos, S. Nie, A. Tsioliaridou, A. Pitsillides, S. Ioannidis, and I. Akyildiz, "A new wireless communication paradigm through software-controlled metasurfaces," *IEEE Commun. Mag.*, vol. 56, no. 9, pp. 162–169, 2018.
- [10] Q. Wu and R. Zhang, "Towards smart and reconfigurable environment: Intelligent reflecting surface aided wireless network," *IEEE Commun. Mag.*, vol. 58, no. 1, pp. 106–112, 2019.
- [11] E. Basar, M. Di Renzo, J. De Rosny, M. Debbah, M.-S. Alouini, and R. Zhang, "Wireless communications through reconfigurable intelligent surfaces," *IEEE Access*, vol. 7, pp. 116 753–116 773, 2019.
- [12] E. Basar, "Transmission through large intelligent surfaces: A new frontier in wireless communications," in *Proc. Eur. Conf. Netw. Commun. (EuCNC)*, 2019, pp. 112–117.
- [13] M. Handley, "Using ground relays for low-latency wide-area routing in

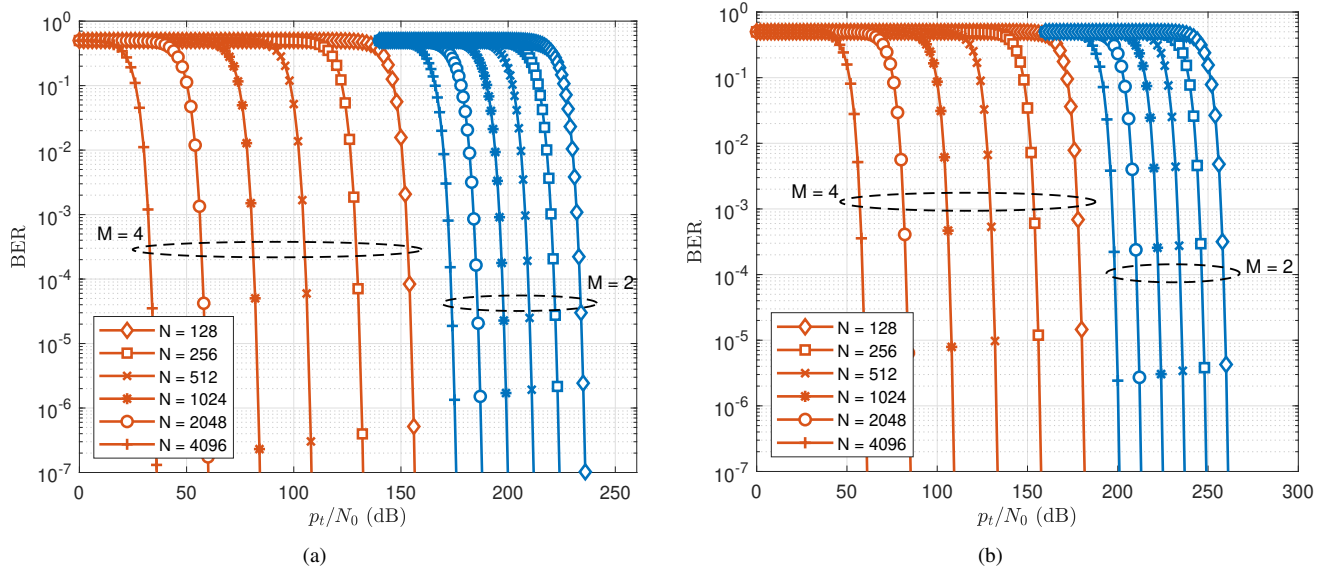


Fig. 13. BER performance for the transmission over consecutive satellites equipped with  $N$ -element RIS on two different constellations: (a) Starlink, (b) Iridium. It should be noticed that all satellites are assumed in the same orbit; thus, the inter-satellite distance is  $d_{intra}$ .

megaconstellations,” in *Proceedings of the 18th ACM Workshop on Hot Topics in Networks*, 2019, pp. 125–132.

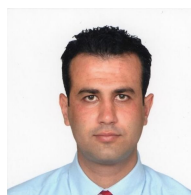
- [14] I. Yildirim, A. Uyrus, E. Basar, and I. F. Akyildiz, “Modeling and analysis of reconfigurable intelligent surfaces for indoor and outdoor applications in 6G wireless systems,” *arXiv preprint arXiv:1912.07350*, 2019.
- [15] M. Handley, “Delay is not an option: Low latency routing in space,” in *Proceedings of the 17th ACM Workshop on Hot Topics in Networks*, 2018, pp. 85–91.
- [16] X. Yang, “Low Earth Orbit (LEO) Mega Constellations: Satellite and Terrestrial Integrated Communication Networks,” Ph.D. dissertation, University of Surrey, 2019.
- [17] A. A. Farid and S. Hranilovic, “Outage capacity optimization for free-space optical links with pointing errors,” *Journal of Lightwave Technology*, vol. 25, no. 7, pp. 1702–1710, Jul. 2007.
- [18] C. A. Balanis, *Antenna Theory: Analysis and Design*. John Wiley & Sons, 2016.
- [19] A.-A. A. Boulogeorgos and A. Alexiou, “Error analysis of mixed THz-RF wireless systems,” *IEEE Commun. Lett.*, vol. 24, no. 2, pp. 277–281, Feb. 2020.
- [20] S. W. Ellingson, “Path loss in reconfigurable intelligent surface-enabled channels,” *arXiv preprint arXiv:1912.06759*, 2019.
- [21] R. Piesiewicz, M. Jacob, M. Koch, J. Schoebel, and T. Kurner, “Performance analysis of future multigigabit wireless communication systems at THz frequencies with highly directive antennas in realistic indoor environments,” *IEEE J. Sel. Top. Quantum Electron.*, vol. 14, no. 2, pp. 421–430, Mar. 2008.
- [22] J. G. Proakis, *Digital Communications*. 4th ed. New York: McGraw-Hill, 2001.
- [23] M. K. Simon and M.-S. Alouini, *Digital Communication over Fading Channels*. John Wiley & Sons, 2005, vol. 95.
- [24] A.-A. A. Boulogeorgos, E. N. Papasotiriou, and A. Alexiou, “Analytical performance assessment of THz wireless systems,” *IEEE Access*, vol. 7, pp. 11 436–11 453, 2019.



**Kürşat Tekbiyık** [StM’19] (tekbiiyik@itu.edu.tr) received his B.Sc. and M.Sc. degrees (with high honors) in electronics and communication engineering from Istanbul Technical University, Istanbul, Turkey, in 2017 and 2019, respectively. He is currently pursuing his Ph.D. degree in telecommunications engineering in Istanbul Technical University. His research interests include algorithm design for signal intelligence, next-generation wireless communication systems, terahertz wireless communications, and machine learning.



**Güneş Karabulut Kurt** [StM’00, M’06, SM’15] (gkurt@itu.edu.tr) received the Ph.D. degree in electrical engineering from the University of Ottawa, Ottawa, ON, Canada, in 2006. Between 2005 and 2008, she was with TenXc Wireless, and Edgewater Computer Systems, in Ottawa Canada. From 2008 to 2010, she was with Turkcell R&D Applied Research and Technology, Istanbul. Since 2010, she has been with Istanbul Technical University. She is also an Adjunct Research Professor at Carleton University. She is serving as an Associate Technical Editor of IEEE Communications Magazine.



**Ali Rıza Ekti** received Ph.D. degree in Electrical Engineering from Texas A&M University in 2015. He is currently an assistant professor at Balikesir University and also senior researcher at TUBITAK BILGEM. His current research interests include statistical signal processing, convex optimization, machine learning, resource allocation and traffic offloading in wireless communications in 4G and 5G systems and smart grid design and optimization.

PLACE  
PHOTO  
HERE

**Ali Görçin** received his Ph.D. degree in University of South Florida (USF) on wireless communications. He worked for Anritsu Company during his tenure in USF and worked for Reverb Networks and Viavi Solutions after his graduation. He is currently holding an assistant professorship position at Yildiz Technical University in Istanbul and also serving as the vice president of TUBITAK BILGEM.



**Halim Yanikomeroglu** [F] (halim@sce.carleton.ca) is a full professor in the Department of Systems and Computer Engineering at Carleton University, Ottawa, Canada. His research interests cover many aspects of 5G/5G+ wireless networks. His collaborative research with industry has resulted in 38 granted patents. He is a Fellow of the Engineering Institute of Canada and the Canadian Academy of Engineering, and he is a Distinguished Speaker for IEEE Communications Society and IEEE Vehicular Technology Society.